NI

NASA Technical Memorandum 81741

Particle and Field Measurements on Two J-Series 30-Centimeter Thrusters

Walter C. Lathem
Lewis Research Center
Cleveland, Ohio

Prepared for the
Fifteenth International Electrical Propulsion Conference
cosponsored by the American Institute of Aeronautics and Astronautics,
the Japan Society for Aeronautical and Space Sciences,
and Deutsche Gesselschaft fur Luft- und Raumfahrt
Las Vegas, Nevada, April 21–23, 1981

NASA

PARTICLE AND FIELD MEASUREMENTS ON TWO J-SERIES 30-CENTIMETER THRUSTERS

by Walter C. Lathem

National Aeronautics and Space Administration
Lewis Research Center
Cleveland, Ohio 44135

INTRODUCTION

A variety of tests have been performed in the past in an attempt to characterize the particles and fields emanating from mercury bombardment ion thrusters. Reference 1 is in essence a compilation and categorization of reported work performed prior to 1979. More recent publications include Refs. 2-7. Reference 3 was the basis for the definition of tests to be performed under the effort reported herein.

All previous efforts were performed with a single thruster and most were performed in smaller facilities which made it difficult to separate facility effects from the thruster particle and field measurements. Also, most tests were performed on early versions of the 30-cm thruster.

This report describes tests performed with two state-of-the-art (J-series) thrusters (ref. 8) operated concurrently in the large (7.6 meter diameter) vacuum facility (ref. 9) at NASA's Lewis Research Center.

Major emphasis was placed on controlling the environment for the tests. Thrusters were operated under computer control to assure stability and repeatability of thruster operational set points. No other tests were permitted to run in the facility while acquiring data to assure stability of the facility background environment. All particle and field data was acquired and recorded under computer control.

A large volume of data was taken during these tests, much of which has not been thoroughly analyzed at the time of this writing. This paper therefore will be limited to a general discussion of the tests performed and those results which appear to have most significance to Solar Electric Propulsion System (SEPS) mission planners. A large portion of the data will be provided for use in a modeling program (ref. 10) used to model the plasma environment surrounding operating ion thrusters.

APPARATUS

Thrusters

The design of the two 30-cm thrusters used in this program (designated J1 and J4) is provided in Ref. 8. The thrusters were mounted as shown in Figure 1. The distance between the thruster axial centerlines was 61 cm.

Power Supplies

The thrusters were operated using functional model power processors designed specifically for use with the J-series thrusters. The power processors are described in Ref. 11.

Thruster Control

Operation of the thrusters was completely controlled by a computer system and a control program described in Ref. 11.

Facility

Thrusters were mounted in a 3.0 m diameter by 3.0 m long test chamber so that the thruster grid plan was within several centimeters of the opening to the 7.6 m diameter by 21.4 m long main vacuum tank at NASA's Lewis Research Center (ref. 9). The facility pressure ranged from 1.1 to 1.7×10^{-6} torr during the tests mainly depending on the level of the thrust beams injected into the facility by the thrusters.

Instrumentation

A variety of diagnostic tools were used for these tests. A brief description of each follows.

Metal deposition tests. - Figure 2 shows the configuration of the two thrusters as viewed from above and also the deposition slide mechanism used for sputtered metal efflux measurements. Shown are both the deployed (test) position and stowed (shielded) position for the slide holders. Figure 3 gives details of the slide holders.

Charged particle efflux tests. - Figures 4-6 show the Faraday Cup/RPA (Retarding Potential Analyzer) sensors used to map the charged particle effluxes for both single and two-thruster operation. Details of the sensors are shown in figure 7. Note the collimating baffle on Polar Probe (POLP) 1 which limited collection of charged particles to a half-angle of approximately 45 degrees.

Floating potential measurements. - Figure 8 shows the sweep pattern of the 2-D rake probe which contain 10 planar potential sensors. Details of the sensor size and locations are shown in figure 9.

Moveable carriage. - The mid thruster fixed probe (MTFP), the azimuthal axial probe (AZAX) and the two dimensional rake probe (2DRP) were all mounted on a carriage which could be moved along the thrust axis a total of 15 cm (fig. 10). Figure 10 shows the axial locations of the AZAX and 2DRP sensors relative to the thruster grid plane for the 4 test positions chosen.

PROCEDURES

Metal Deposition Tests

Calibration run. - A calibration run was initially made to determine the amount of material deposited on the test slides in the stowed position. During this run an unscheduled tank shutdown occurred after 258 hours.

During this test period the following conditions prevailed:

1) facility pressure range was 8.5×10^{-7} to 1.5×10^{-6} torr (1.1 to 2.0×10^{-4} Pascals)

2) thruster J1 logged 224 ampere-hours

3) thruster 702 (upgraded to J-series thruster specifications) logged 124 ampere-hours in the J-4 mounting position)

4) an on-going cathode life test was located 10.4 meters downstream of the J-series thrusters. During this calibration run the cathode life test logged 119 hours.

The quartz test slides and a reference slide cleaned at the same time prior to test were removed and spectrally analyzed and compared to a sample of Convoil 20 oil used in the diffusion pumps. The main conclusion of the test was that an insignificant amount of oil had reached the slides even though the unscheduled tank shutdown created a situation where oil backstreaming probably occurred. No evidence of metal deposition from tank sputtering was observed in the stowed position. This resulted in greater confidence in the cleanliness of the test slides when first deployed.

Deployed position test. - Following the calibration run the tests slides were deployed and exposed to the beam of thruster J4 running at 2.0 Amps beam current (fig. 2). After the test, the quartz slides were removed, and the spectral transmittance at wavelengths of 840 and 1000 angstrom was measured using an integrating sphere-monochromator (ref. 12). Using the technique described in reference 12, the arrival rate of sputtered material at each slide location was then calculated.

Thruster Stabilization and Data Acquisition

For each thruster condition a number of steps were taken to assure data reliability. After a thruster startup an overnight stabilization was allowed before taking data. A waiting period of from 1 to 3 hours was observed following a throttle from one operating point to another. Although the data was taken automatically under computer control, the data was also displayed real-time on a CRT and monitored visually by the operator. A full set of thruster electrical data was taken every 15 minutes and a complete set of mercury propellant flow readings taken for each test condition.

Floating Potential Measurements

The current collected by the sensors of the 2DRP probe was passed through an 11 megohm resistor and the resulting voltage drop measured and recorded. For the Faraday Cup/RPA sensors, all grids were tied together electrically and the current collected by the outer grid passed through an 11 megohm resistor as for the 2DRP.

Charged Particle Efflux Measurements

These were made using the Faraday Cup/RPA sensors. The suppressor grid was held at -20 volts to preclude secondary electron emission from the collector. The outer grid was set to a voltage 0.3 volts above the floating potential measured previously in an attempt to have the outer part of the

box close to plasma potential. An average electron temperature of 0.3 eV was assumed. The retarding potential was then varied from -20 to 86 volts and the resulting current to the collector was recorded. The effective collection area of these sensors was ~35 cm^2.

RESULTS AND DISCUSSION

Metal Deposition Tests

Thruster J4 was operated for 332 hours at a 2.0 ampere beam current with the probe in deployed position. Results are shown in figure 11. The deposit growth rate was calculated using the techniques described in reference 12. In figure 11 the data are compared with a theoretical calculation using the equations of reference 13. A sputtering yield of 1 atom per ion was assumed in the calculation. The net deposition growth rate on the slides at angles from 45° to 60° from the thrust axis are greatly reduced due to direct ion sputtering by high energy ions. That is, metal is being deposited and simultaneously removed by sputtering of high energy beam ions. Note that the growth rate is non-zero at 90° as was found with results of reference 12.

Charged Particle Efflux Measurements

A calibration run was performed with no thrusters running in the facility. A complete RPA analysis in which the retarding potential was varied from -20V to +86V was performed for each of the four sensors at predetermined locations as follows. Locations for the Polar Probe (POLP) were measured for polar angles (θ), see figure 6, every 10° from 70° to 270°. As shown in figure 5, locations for the azimuthal axial probe were measured for angles of ϕ every 10° from 90° to 270° relative to the centerline of the probe rotation. This corresponds to azimuthal angles (ϕ) of 103° and 257° respectively. As shown in Table I all collected currents were of the order of nanoamps. Also shown is the data taken with the Two Dimensional Rake Probe (2DRP) every 3° from 0° to 360°, figure 8. The floating potentials measured ranged from 0.055 to 0.102 volts. Data for the mid thruster fixed probe (MTFP) were taken only at one carriage position, position A of figure 10. Results are shown in Table I.

Table II shows the 10 thruster operating conditions for which a complete set of diagnostics were run. The table shows the beam current for each thruster and the order (see data) in which tests were performed. Note that the tank pressure for all tests was between 1.1 and 1.7×10^{-6} torr. Complete flow data was taken and is shown in the table in equivalent milliamperes of mercury. The neutralizer keeper voltage (Vnk) was included because the power processor for thruster J1 was malfunctioning and not able to repeat the same value of Vnk. Compare, for example, tests 4A and 4B where Vnk was controlled to two different values by the power processor forthe same set point command. It should be noted however that once the condition was set, the set point was maintained within normal limits.

MTFP. - The Mid Thruster Fixed Probe (see fig. 4) was located between the two thrusters but above the x-z plane approximately 23 cm. Data was taken at four z-axis (thrust axis) locations: -3.2 cm (upstream of the grid plane) and +1.9, +7.0 and +12.1 cm (downstream). Results are shown in

figure 12 plotted as total sensor collector current versus total beam current (both thrusters) for the four z-axis locations. Data is presented in this way to indicate the extent to which one can extrapolate single thruster data to two thruster data. It is noted that the collector current is almost identical with either of the two thrusters running independently. When both thrusters are running however, there is some increase in the collector current for the same total beam current.

The data of figure 12 were taken at a retarding potential of zero volts. The data therefore represents the total flux entering the probe at all energies. By varying the retarding potential it was found that at 6.3 volts the collector current dropped two orders of magnitude and at 9.6 volts the current collected was negligible. Thus it was concluded that all particles entering the collector had energies less than 6-10 electron volts.

POLP. - The Polar Probe has two sensors, (figures 6 and 7). The sensor facing the thrusters will be referred to as POLP 1 and the sensor facing away from the thrusters as POLP 2. Note the baffle on POLP 1 in figures 6 and 7. Results from these two sensors will be presented together. The general objective of POLP 2 was to measure the flux of charged particles in an upstream direction. It was postulated that such particles would be formed by charge exchange between neutral mercury which has been sputtered from the tank walls and ions in the primary ion beam. These particles, it was theorized could enter the sensors which have a view of the beam and thus give an artificially high reading.

Figure 13 shows results of tests 4B, 5B and 6B (see Table II). Only thruster J1 was running. As expected, the current collected by POLP 2 was several orders of magnitude below POLP 1 in the central region of the facility. The POLP 2 signal was about 10^{-7} amps for all beam currents in this region. It is not known whether the bulge in the very center (only single point spikes for 0.75 and 1.30 A) is real or an interaction of some kind between the back-to-back sensors.

The current collected by POLP 2 falls off on either side of the facility centerline (180^{0}) partially due to the radial variation in beam density but also due to the decreasing view factor of the sensor. The sensor was fixed on the end of the probe arm and thus was perpendicular to the facility centerline at 180^{0} while it was parallel to the centerline at 90^{0} and 270^{0}.

The data of figure 13 for POLP 1 clearly show the "edges" of the beam at 110^{0} and at 230^{0} with respect to facility centerline. Note that the sensor was on the J1 thruster centerline at 165^{0} and on the J4 thruster centerline at 195^{0}. Keeping in mind that the sensor was at a different distance from thruster J1 at 110^{0} and 230^{0} and also had a slightly different viewing angle, it can be concluded from the data that the primary beam of thruster J1 had a half angle of about 60^{0}. This is consistent with results of the deposition tests discussed earlier (fig. 11), where the deposit growth rate decreased significantly at the edge of the beam.

A similar plot of thruster J4 data (not included herein) showed a near mirror image of the data of Figure 13 for POLP 1. The base data for POLP 2

was about 10^{-7} amps consistent with Figure 13. The spikes were in different locations for J4 but in general the data exhibited the same characteristics for both thrusters.

Figure 14 shows results of two thruster operation with both at 2.0 A and at 0.75 A beam current. Just as with the single thruster case, the POLP 2 current appears to be at the general level of 10^{-7} A. Because this data exhibits higher and more random spikes the suspicion is that the highly noisy environment is causing some difficulty for the decade auto-ranging amplifiers used with these sensors. For example, many of the points of figure 14 that are above 10^{-7} amps would appear to fit the general curve almost exactly, merely by plotting them a decade lower.

The data of figures 13 and 14 were taken with a zero volt retarding potential. Thus the data represents total ion flux at all energies. Figure 15 shows a typical case of retarding potential analysis of thruster J4 at 0.75 A beam current using POLP 1. Note that at probe angles of 150^{0} (fig. 15(a)) and 230^{0} (fig. 15(b)) the constancy of the data at all potentials indicates that nearly all of the current is made up of the primary beam ions with perhaps some part of it being ions with energies ranging from 100 volts to 600 volts (net accelerating potential was 600 volts). At angles further away from the facility centerline the range in low energy particle fluxes becomes apparent.

The data at 90^{0}, 110^{0} and 270^{0} indicate that there is a flux of ions with energies greater than 86 volts. While the signal is only about 3×10^{-9} A at 90^{0} and 270^{0}, this is still higher than the base readings taken with no thrusters operating (see Table I). While it is difficult to precisely define the origin of these higher energy particles it should be noted that a baffle was placed around POLP 1 (figs. 6 and 7) to restrict the view factor of the sensor to a half angle of about 45^{0} or so. This makes it seem unlikely that the particles are "facility effect" ions. To place things in proper perspective, the 3×10^{-9} A of current is only approximately 1×10^{-10} A/cm^{2}. At 270^{0} the radial distance from the thruster J4 beam edge to the sensor was approximately 75 cm while at 90^{0} the distance was approximately 135 cm. At this latter location the sensor was looking across the face of thruster J1 (which was not running in this case).

A direct comparison of the data for 90^{0} and 270^{0} shows a reduced flux at 90^{0} for the lower retarding potential values. This might indicate that some of the lowest energy particles were being intercepted by the J1 thruster whereas the higher energy particles are able to clear that structure and arrive at the sensor.

The energy spectrum of backstreaming ions as detected by POLP 2 is shown in figure 16 for thruster J1 at 0.75 A beam current. The data for zero volts retarding potential are the same as plotted in figure 13. Most of the ions are repelled by 9.6 volts retarding potential in the center of the facility. At angles further from the facility centerline, i.e., greater than 220^{0} or less than 110^{0} the ions are repelled by only 3.1 volts energy. This would indicate that the energy as well as the flux density decreases with increasing radial distance from thrust axis. This result was not unexpected.

AZAX. - Data from the azimuthal axial sensor was considered valuable because it was intended to map the particle fluxes flowing radially outward from the thrusters in directions which might intercept parts of the spacecraft, i.e., angles of 90° or so from the thrust axis. The actual survey area was limited to the range 86° to 92° in the x-z plane (see Fig. 6) due to limited translation of the carriage in the z-direction. The locations A through D from figure 10 represent polar angles (θ) of 86°, 88°, 90° and 92° respectively.

Figure 17 compares data for the A and D positions for two different thruster operating conditions. As expected the variation in collector current for a given operating condition is small due to the small change in sensor location. Also, as expected, the current collected was higher in the D position for all thruster conditions.

The data of figure 17, and of all subsequent AZAX figures were plotted as a function of the azimuthal angle (φ) of figure 5 with the origin midway connecting the centers of the thrusters. The mechanical limit of travel in the x-y plan of figure 5 was 103° on one side and 257° on the other. Data from POLP 1 (fig. 6) were added to figure 17 for values of the polar angle θ corresponding to the A and D positions of the AZAX, i.e., 86° and 92° respectively. These points are shown as shaded points in figure 17. Considering the fact that the POLP 1 sensor had a baffle (figs. 6 and 7) and the AZAX did not, the data is in good agreement. In fact, if facility effect ions are indeed entering the AZAX the flux density must be pretty small.

Also shown in figure 17 are the POLP 2 signals for the same locations (90° and 270°). The signal level is several orders of magnitude less than for AZAX and POLP 1. The AZAX and POLP 2 were at approximately the same radial distance from the beams and both collectors were parallel to the thrust axis. The only difference was they were oriented in opposite directions. This would seem to further support the conclusion that the bulk of the AZAX signal is in actuality thruster produced ion flux rather than facility effect ions.

Results of retarding potential analysis for test 7 with both thrusters at 2.0 A is shown in figures 18 and 19. Figure 18 shows the variation of sensor current with retarding potential with the probe in position D. While the majority of ion flux is made up of energies less than 10 volts or so there seems to be a continuous spectrum of energies up to the 87 volt level (the limit of the retarding potential supply). Note that the flux of particles having energies greater than 87 volts is of the order of 10^{-7} amps compared with the calibration results of ~10^{-9} A (Table I). Again, data from POLP 1 is in good agreement with AZAX data.

For comparison, figure 19 shows similar data with the probe in position A. On the right side of the figure, at φ = 90°, the POLP 1 data again agrees with AZAX data. Equivalent data for the left side, at φ = 270° could not be obtained because mechanical limits prevented the POLP from traveling upstream of the plane of the grids on that side so that it could be positioned in the x-y pland of the AZAX. This was unfortunate in light of the unexpected behavior shown in the left half of figure 19 at energies

greater than 19.3 volts. Data for other thruster operating conditions were plotted and this behavior was still exhibited.

Figure 20 shows results for the AZAX similar to the MTFP data of figure 12. The total collector current is plotted as a function of total beam current (both thrusters) for each of the four axial probe locations and for all 10 operating conditions of Table II. The location of the probe was at $\phi = 180^0$, figure 5.

Floating Potential Measurement

These measurements were not intended to obtain a detailed, highly accurate mapping of the potential fields and gradients in the vicinity of operating ion thrusters. Rather they were intended to determine the general shapes of the potential profiles and to estimate the maximum and minimum potentials as inputs for thruster plume modeling.

2DRP. - The two dimensional rake probe, outfitted with ten sensors was used to sweep out a plane parallel to the thruster grids (figs. 8 and 10). Table III summarizes the maximum and minimum floating potentials measured over an azimuthal scan of $\phi' = 360^0$ for each of the ten thruster operating conditions of Table II and each of the four axial positions of figure 10.

As expected, the maximums were measured in the primary ion beam region. For all operating conditions there was a relatively flat area about the size of the grids (30 cm diameter). The average potential varied less than about 0.3 volts in this region. Also, as expected the size of the flat area increased with increasing axial distance from the grids. Figure 21 shows contour maps at the four axial locations for operating condition 7, i.e., both thrusters at 2.0 A. Note the rapid falloff of potential near the neutralizer. Also noted, but not understood, was the difference in falloff above and below the two thrusters.

The negative values of Table III should only be used in a qualitative way. The minimum values occurred repeatedly in the vicinity of the neutralizer. The outermost sensor which was 45 cm from the axis of probe rotation passed directly over the neutralizers and data was taken every 2-2.5 cm of travel. Therefore, a data point would not necessarily be taken directly over the neutralizer but could be as much as a centimeter or so off line. In fact, no attempt was made to synchronize the data sampling in this way. As a result, the negative potential sampled would have considerable scatter.

The general characteristics of the profiles of figure 21 were consistent for all thruster operating conditions.

CONCLUSIONS

Tests have been performed to characterize partially the particles and fields associated with two state-of-the-art (J-series) 30 cm diameter mercury ion thrusters operating independently and simultaneously.

The flux rate of sputtered metal atoms leaving a single thruster has been determined. The data show agreement with tests for previous versions of the 30-cm thruster.

The flux rate and energies of ions leaving single and two-thruster configurations has been determined to a degree sufficient to establish at least upper bounds. This data was determined for a variety of beam current levels and combinations for the two thrusters.

The flux rate and energies of facility effect ions was measured. Flux rates were sufficiently small that in most cases only 2nd and 3rd order corrections to other measurements are necessary.

Floating potential measurements were made which indicate that the fields in the near vicinity of the thruster are very weak, i.e., ± a few volts.

In summary, it is believed that sufficient data have been presented to allow SEPS mission planners to estimate the level of neutral and in flux at least to first order so that impact on other spacecraft components may be assessed.

REFERENCES

1. Byers, D. C., "Electron Bombardment Thruster Field and Particle Interfaces," Journal of Spacecraft and Rockets, Vol. 16, Sept.-Oct. 1979, pp. 289-301.

2. Carruth, M. R., Jr. and Brady, M. E., "Propogation of Charge-Exchange Plasma Produced by an Ion Thruster," AIAA Paper 80-1388, July 1980.

3. Komatsu, G. K., "Particle Efflux and Fields Test Definition, " TRW Defense and Space Systems Group, Redondo Beach, CA, REPT-32827-6024-RU-00, Sep. 1979, (NASA CR-159704).

4. Carruth, M. R., Jr. and Kuo, Y. S., "Ion Thruster Plume Effects on Spacecraft Surfaces," AIAA Paper 80-1228, June 1980.

5. Kaufman, H. R., "Plasma Physics Analysis of SERT II Operation," Colorado State Univ., Fort Collins, CO, Jan. 1980, (NASA CR-159814).

6. Kaufman, H. R. and Carruth, M. R., Jr., "Charge-Exchange Plasma Environment for an Ion Drive Spacecraft," Jet Propulsion Lab., California Inst. of Tech., Pasadena, CA, JPL-Pub-79-90, Oct. 1979.

7. Whittlesey, A. C., "Electromagnetic Interference Assessment for an Ion Drive Electric Propulsion System," AIAA Paper 79-1328, June 1979.

8. Bechtel, R. T., "The 30 Cm J-Series Ion Thruster," AIAA Paper 81-0714, Apr. 1981.

9. Finke, R. C., Holmes, A. D., and Keller, T. A., "Space Environment Facility for Electric Propulsion Systems Research," NASA TN D-2774, 1965.

10. Katz, I., Parks, D. E., Mandell, M. J., and Schneulle, G. W., "Parasitic Current Losses Due to Spacecraft Generated Plasmas," AIAA Paper 81-0740, Apr. 1981.

11. "30-Centimeter Ion Thrust Subsystem Design Manual," NASA TM-79191, 1979.

12. Weigand, A. J. and Mirtich, M. J., "Measurement of Sputtered Efflux From 5-, 8-, and 30-Cm Diameter Mercury Ion Thrusters," AIAA Paper 75-358, Mar. 1975.

13. Kemp, R. F., Miller, W. D., Luedke, E. E., and Hall, D. F., "Effects of Electrostatic Rocket Material Deposited on Solar Cells," AIAA Paper 72-447, Apr. 1972.

TABLE I. - CALIBRATION RUN -- NO THRUSTERS RUNNING

	Angles	RETARDING Potential, V	TOTAL Current, 10^{-9} A
POLP 1	All values	All values	-2.5
POLP 2	70, 80, 270	All values	-4.0
	100 to 260	<6.4	-1.8 to -4.0
		>6.4	-4.0
AZAX	All values	0	0.88 to 1.04
		>3.2	0.55 to 0.60
MTFP	NA	0	1.8
		>3.2	-1.5 to -35.0
2-DRP	Floating potential 0.055 to 0.102 V (Data recorded every 3^{0} from 0^{0} to 360^{0})		

TABLE II. – PARTICLES a FIELDS
TEST MATRIX

Test	Probes				J-4					J-1					P_{tk}	DATE
	POLP	AZAX	MTFP	ZDRP	EQV. NEUT. FLOW RATE					EQV. NEUT. FLOW RATE						
					J_b	$\dot{n}_{\square}$	$\dot{n}_c$	$\dot{n}_n$	V_{nk}	J_b	$\dot{n}_{\square}$	$\dot{n}_c$	$\dot{n}_n$	V_{nk}	10^{-6}	
					A	nA	nA	nA	V	A	nA	nA	nA	V	Torr	
1A	X	X	X		.75	784	117	39	14.6						1.3	10/3
1B				X	.75	—	—	—	14.6						1.4	10/7
1C	X	X	X	X	.75	778	122	44	14.6						1.3	10/22
2A	X	X	X		1.28	1325	99	35	13.6						1.4	10/3
2B				X	1.28	—	—	—	13.6						1.4	10/7
2C	X	X	X	X	1.28	1322	102	40	13.6						1.3	10/23
3A	X	X	X		2.01	2089	84	30	13.6						1.5	10/3
3B				X	2.01	—	—	—	13.6						1.7	10/5
3C	X	X	X	X	2.01	2086	87	31	13.6						1.3	10/23
4A	X	X	X							.74	783	102	53	14.5	1.5	10/2
4B	X	X	X	X						.74	783	108	43	15.0	1.1	10/17
5A	X	X	X							1.27	1310	88	31	14.6	1.6	10/1
5B	X	X	X	X						1.27	1310	94	32	14.9	1.2	10/20
6A	X	X	X							1.96	1974	75	34	13.6	1.5	10/1
6B	X	X	X	X						1.96	1987	83	32	14.0	1.3	10/21
7	X	X	X		2.01	2059	81	29	13.6	1.96	1971	73	30	13.6	1.6	9/29
7A				X	2.01	—	—	—	13.6	1.96	—	—	—	13.4	1.6	10/21
7B	X				2.01	—	—	—	13.6	1.96	—	—	—	13.4	1.5	10/22
8	X	X	X		2.01	2075	85	34	13.6	.74	784	102	50	14.5	1.6	9/30
8A				X	2.01	—	—	—	13.6	.74	—	—	—	15.4	1.4	10/21
8B	X				2.01	—	—	—	13.6	.74	—	—	—	15.4	1.3	10/22
9	X	X	X		.75	784	121	39	14.6	.74	781	100	48	14.5	1.5	9/30
9A				X	.75	—	—	—	14.6	.74	—	—	—	15.4	1.2	10/21
9B	X				.75	—	—	—	14.6	.74	—	—	—	15.4	1.2	10/22
10A	X	X	X		.75	782	117	33	14.6	1.96	1964	73	32	13.6	1.6	10/1
10B	X	X	X	X	.75	774	120	44	14.6	1.96	1981	82	44	13.6	1.4	10/22

TABLE III. - FLOATING POTENTIALS (VOLTS) FOR 10 THRUSTER OPERATING CONDITIONS AT FOUR AXIAL LOCATIONS DOWNSTREAM OF THRUSTERS

Thruster	Test Condition (Table II)	Axial Locations of Figure 10							
		A		B		C		D	
		Max	Min	Max	Min	MAX	MIN	MAX	MIN
J4	1	1.5	-3.2	1.4	-3.6	1.4	-3.0	1.4	-1.9
	2	2.3	-5.0	1.6	-5.0	1.6	-4.2	1.5	-3.4
	3	2.3	-6.7	1.9	-7.2	1.9	-7.0	1.6	-1.7
J1	4	1.3	-4.3	1.2	-4.4	1.2	-4.4	1.1	-4.5
	5	1.7	-6.2	1.7	-6.1	1.6	-5.4	1.6	-5.1
	6	2.2	-7.2	2.1	-7.8	2.0	-6.9	2.0	-5.9
Both	7	1.8	-6.3	1.8	-7.4	1.7	-6.8	1.7	-5.6
	8	2.1	-7.4	1.8	-7.3	1.7	-6.7	1.7	-5.4
	9	1.4	-4.6	1.4	-4.5	1.4	-3.8	1.3	-2.9
	10	1.8	-6.1	1.7	-6.5	1.7	-6.3	1.7	-4.4

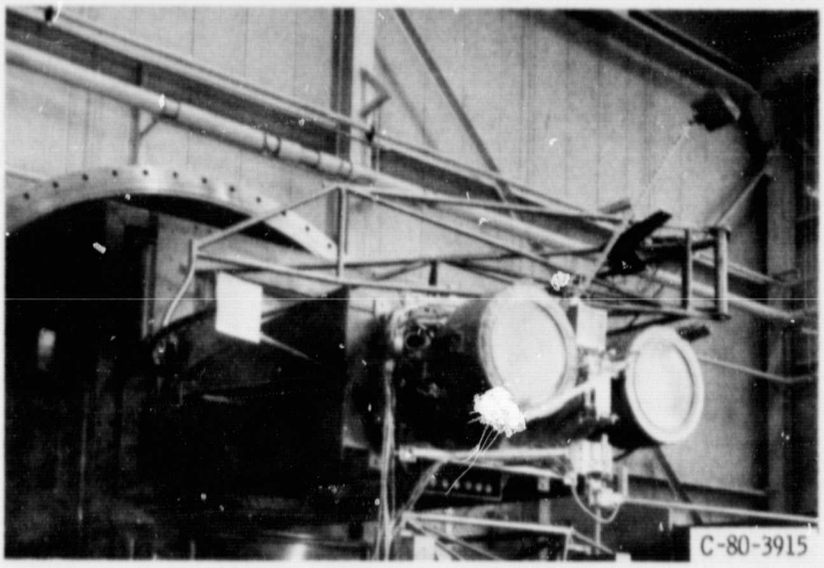

Figure 1. - Two J-series thrusters and diagnostics ready for test in large facility at LeRC.

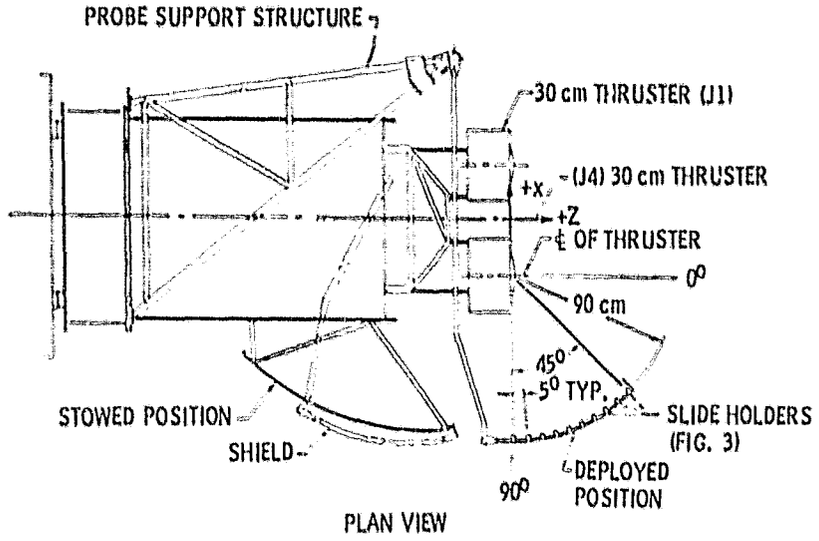

Figure 2. - Deposition slide test configuration.

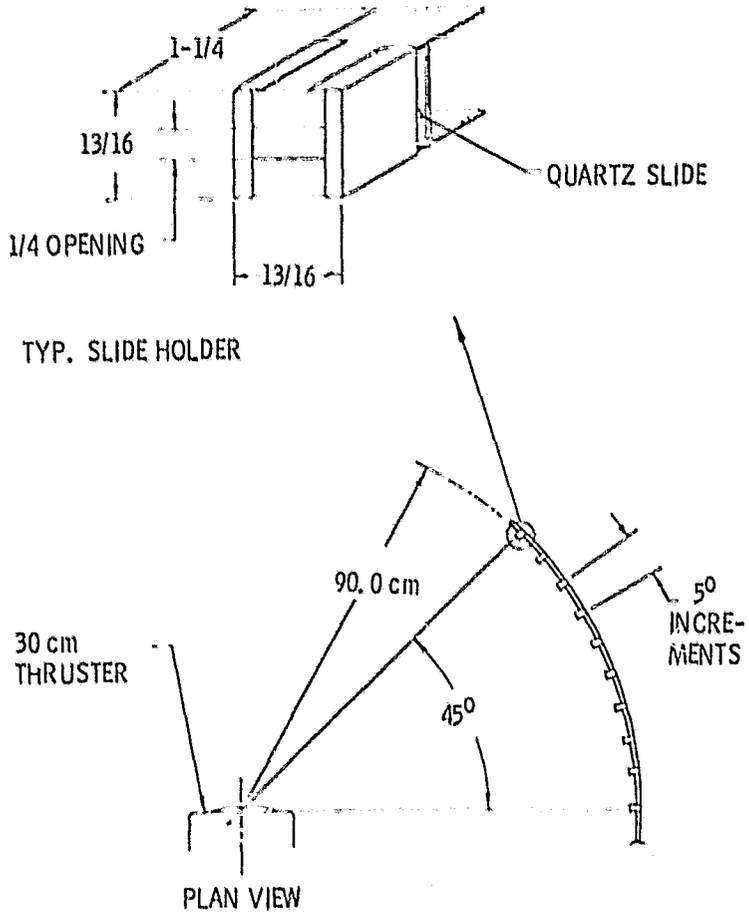

Figure 3. - Metal deposition test setup.

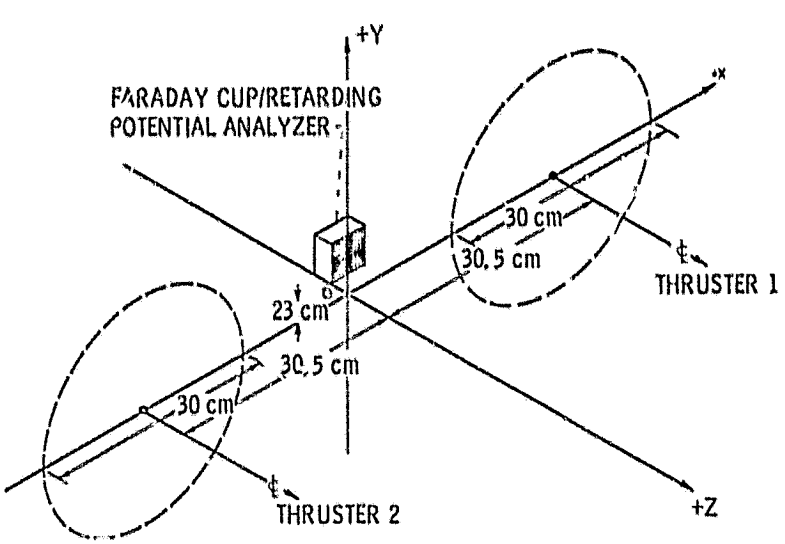

Figure 4. - Two thruster coordinate system showing location of mid thruster fixed probe (MTFP).

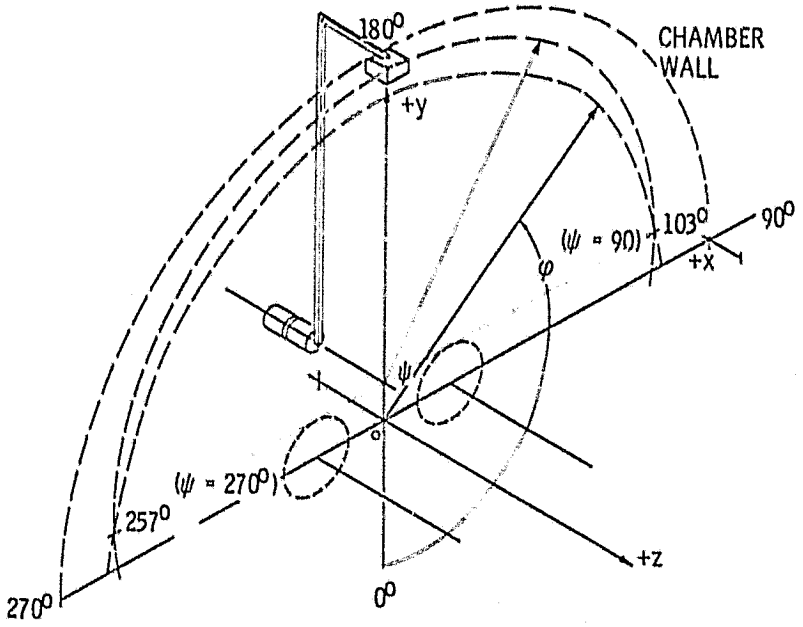

Figure 5. - Azimuthal axial probe (AZAX).

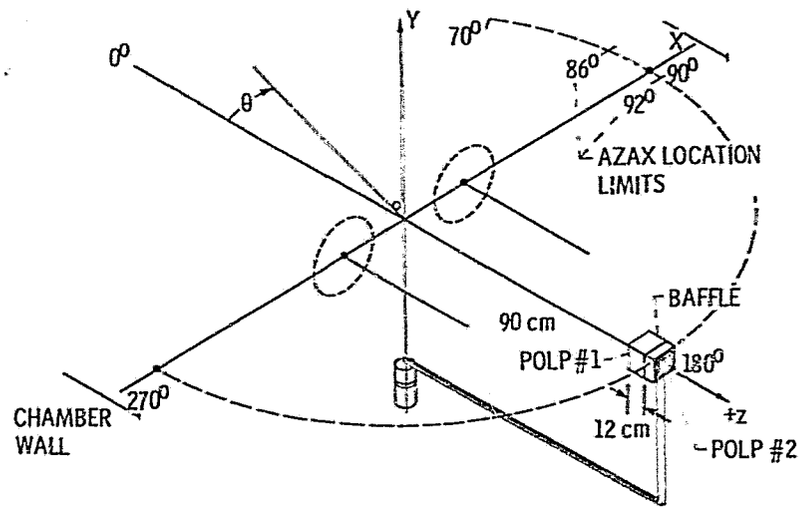

Figure 6. - Polar probe (POLP) with back to back sensors.

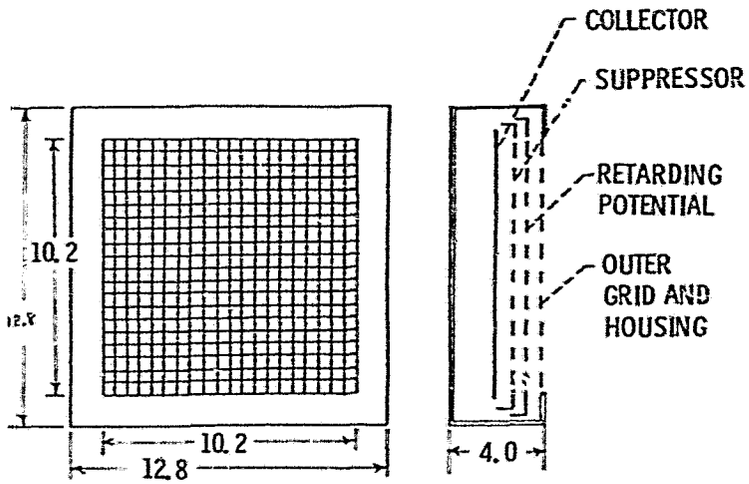

(a) Front view of all sensors and side view of AZAX and MTFP.

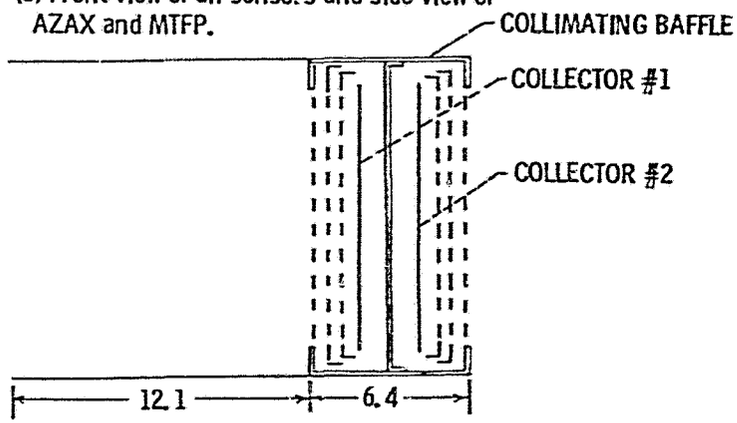

(b) Side view of POLP with two collectors and baffle.

Figure 7. - Front and side views of Faraday Cup/RPA sensors. Dimensions in centimeters.

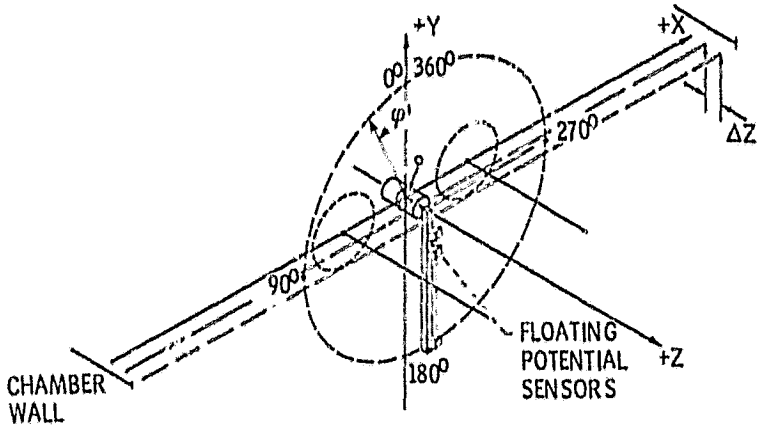

Figure 8. - Two-dimensional rake probe (2 DRP) for potential measurements.

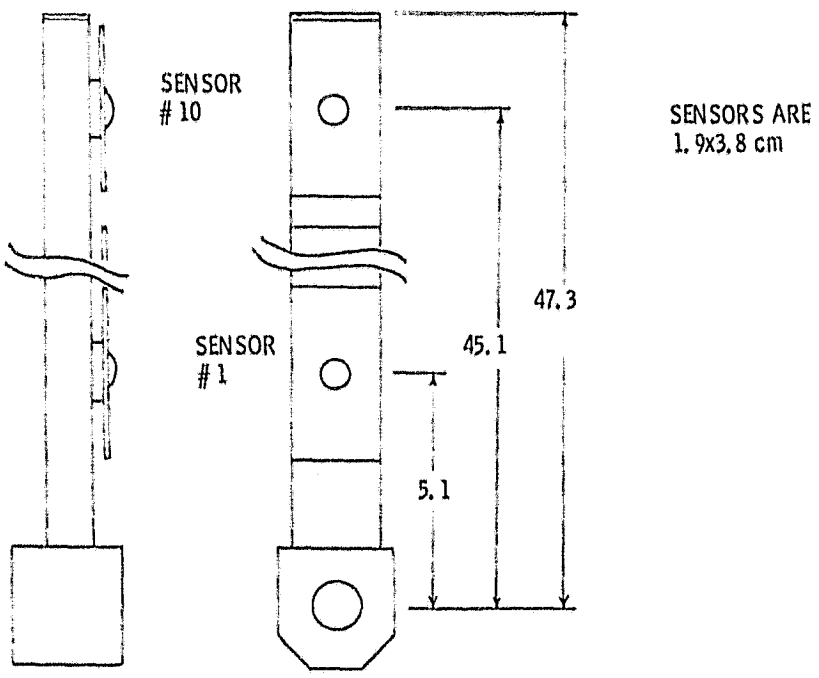

Figure 9. - 2 DRP Floating potential sensors. Dimensions are in cm.

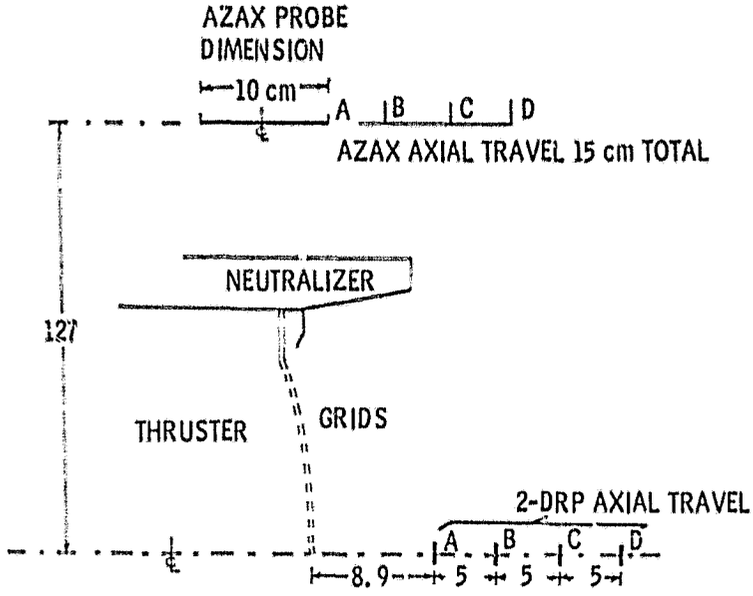

Figure 10. - Relative location of AZAX and 2 DRP with respect to grid plane for test locations A-D. Dimensions in cm.

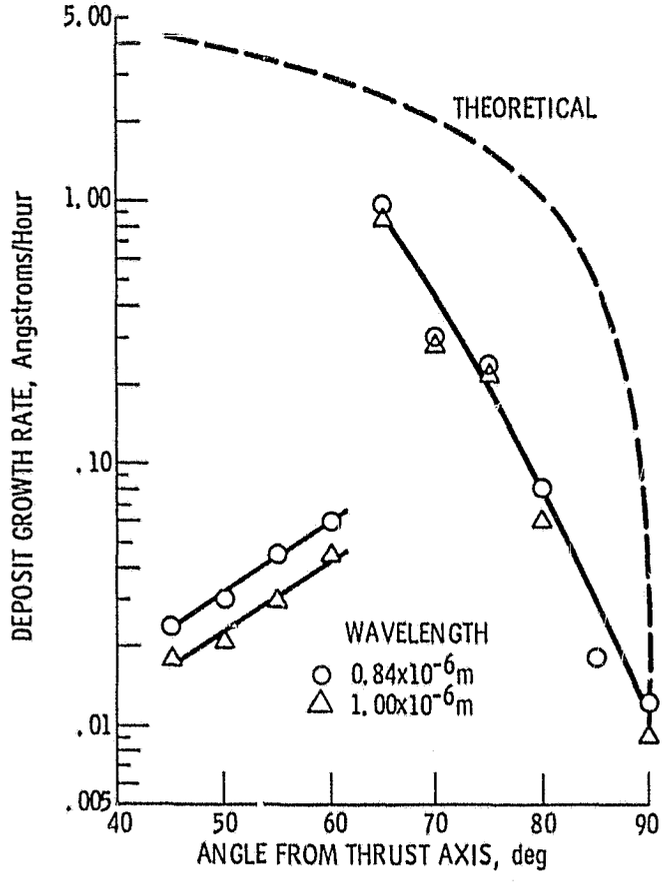

Figure 11. - Deposit growth rate of ion sputtered metal as a function of angle from thrust axis at a radial distance of 90 cm. J_B = 2 amperes.

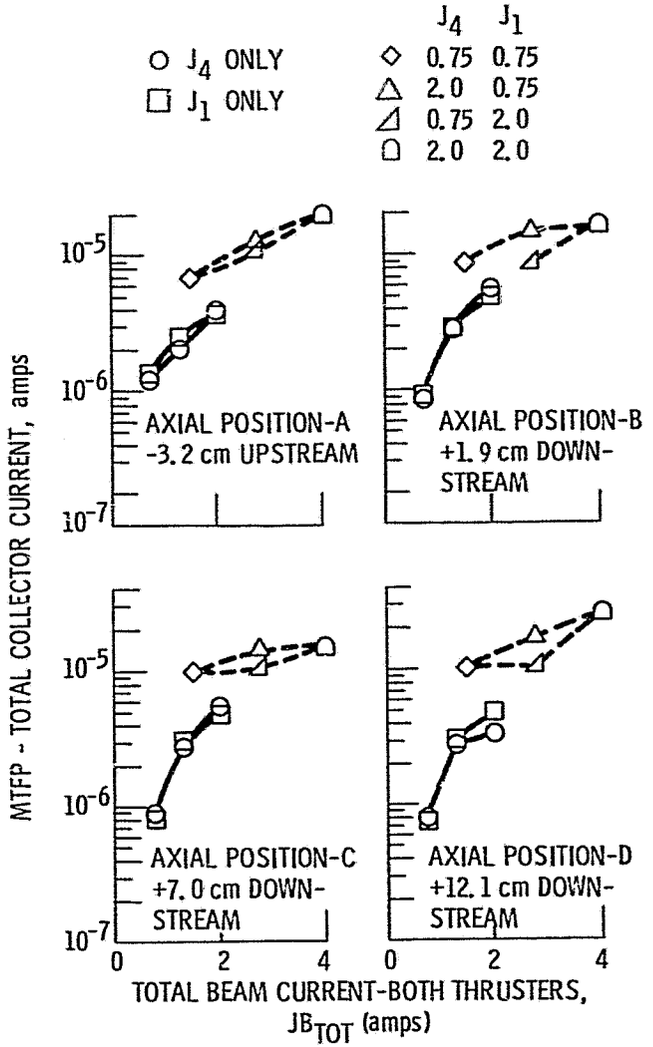

Figure 12. - Total current collected by MTFP as a function of total thruster beam, current for four axial locations.

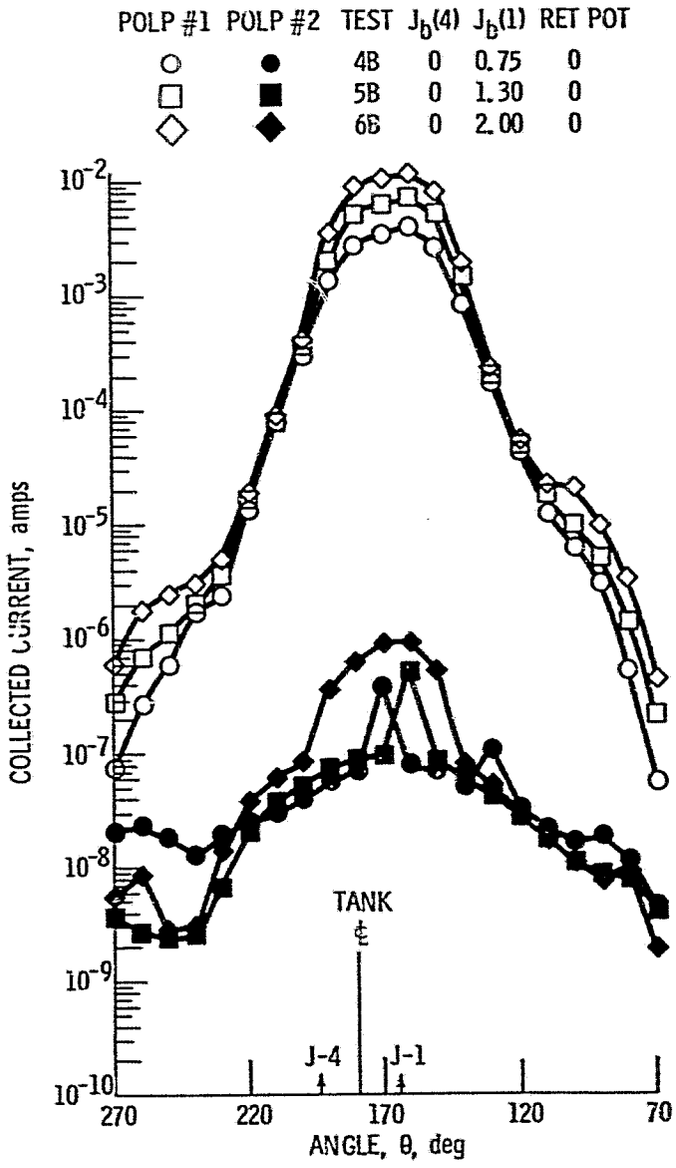

Figure 13. - Total current collected by POLP #1 and POLP #2 as a function of angle θ (see fig. 6).

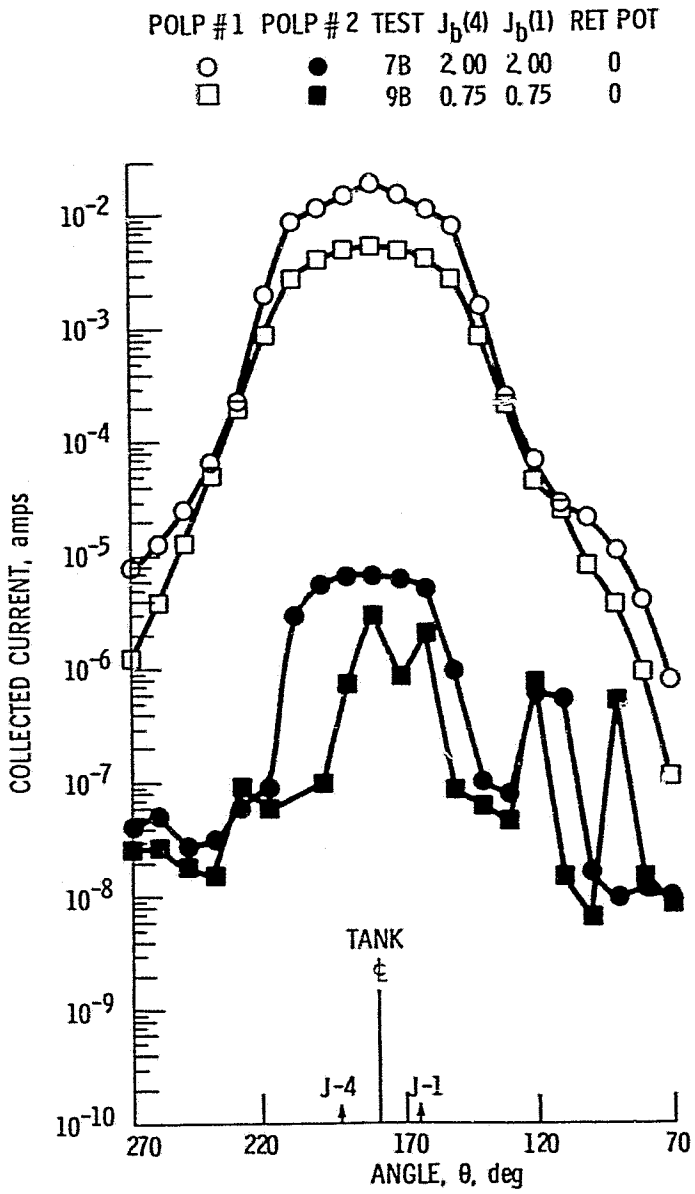

Figure 14. – Total current collected by POLP # 1 and POLP # 2 as a function of angle θ (see fig. 6).

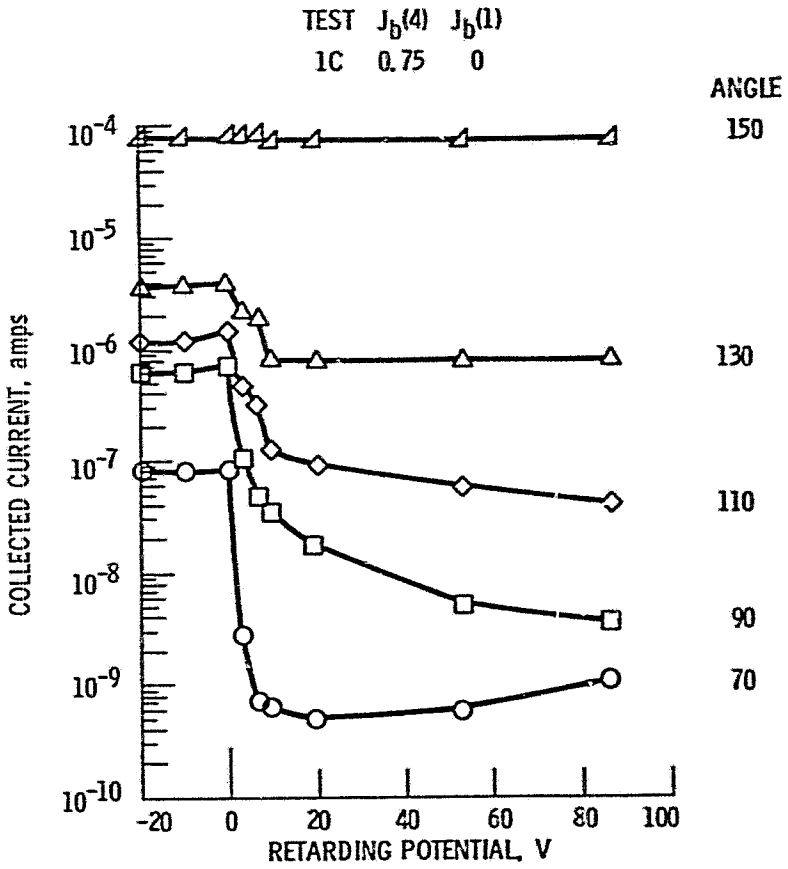

Figure 15(a). – Current collected by POLP # 1 as a function of retarding potential for various values of angle θ (see fig. 6).

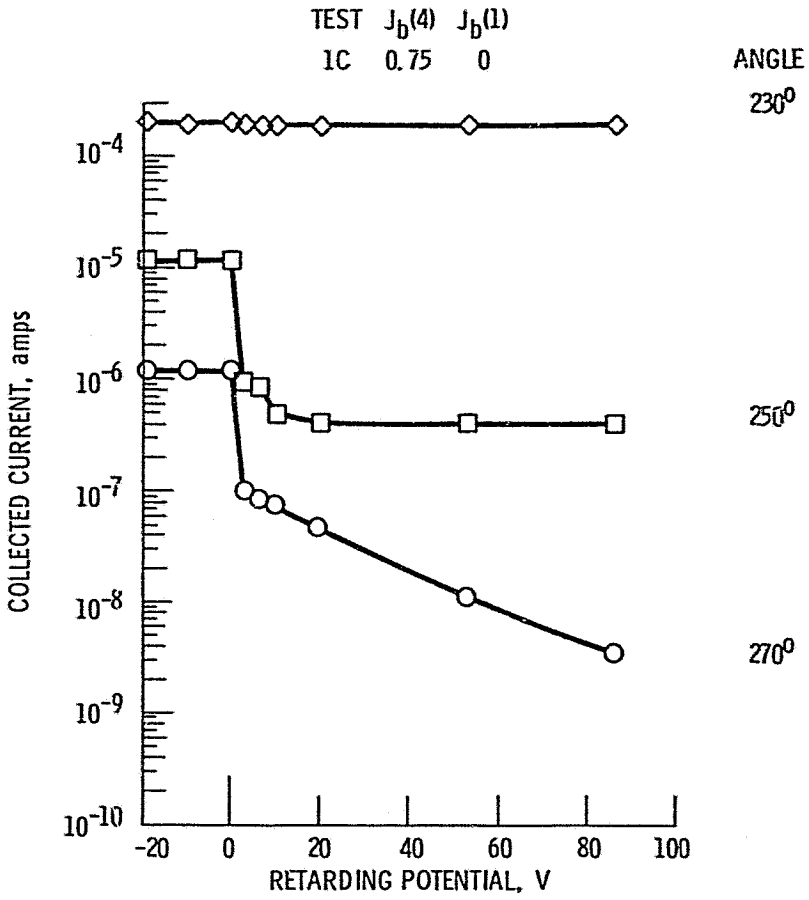

Figure 15(b). - Current collected by POLP #1 as a function of retarding potential for various values of angle θ (see fig. 6).

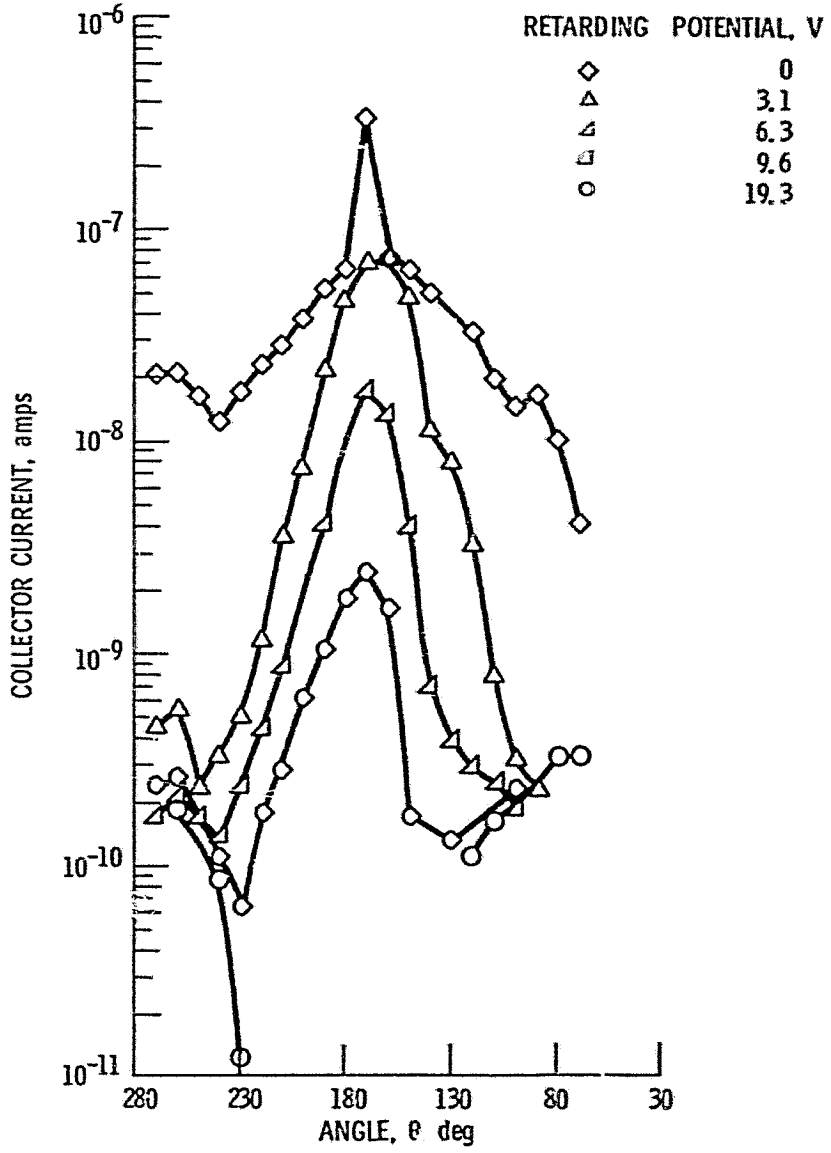

Figure 16. - Collector current for POLP #2 as a function of angle θ (see fig. 6) for various retarding potentials.

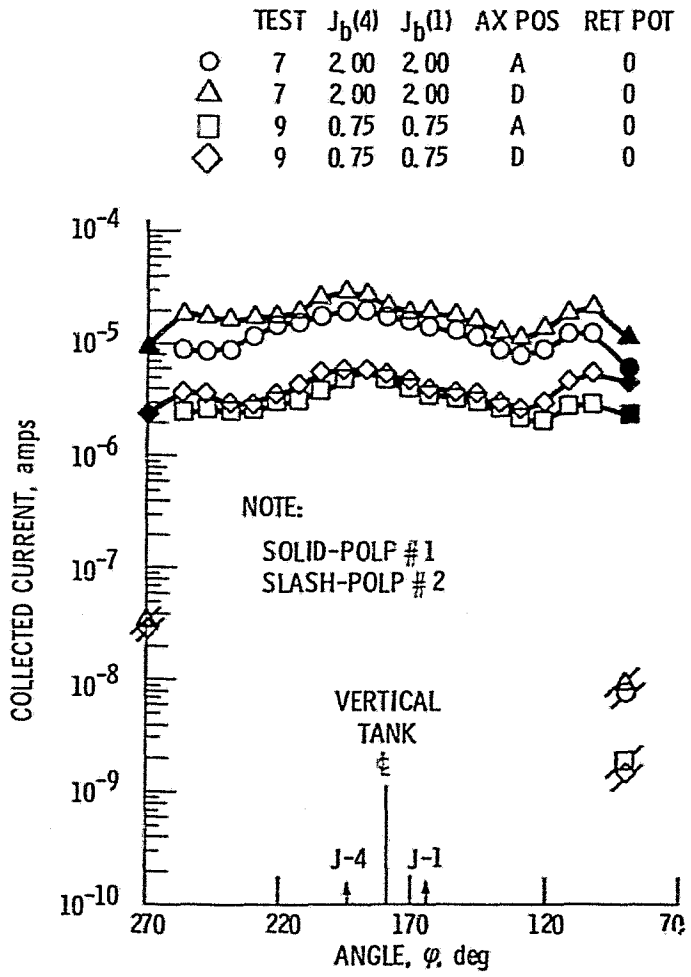

Figure 17. – Current collected by AZAX as a function of angle φ (see fig. 5) for two axial positions and two thruster operating conditions.

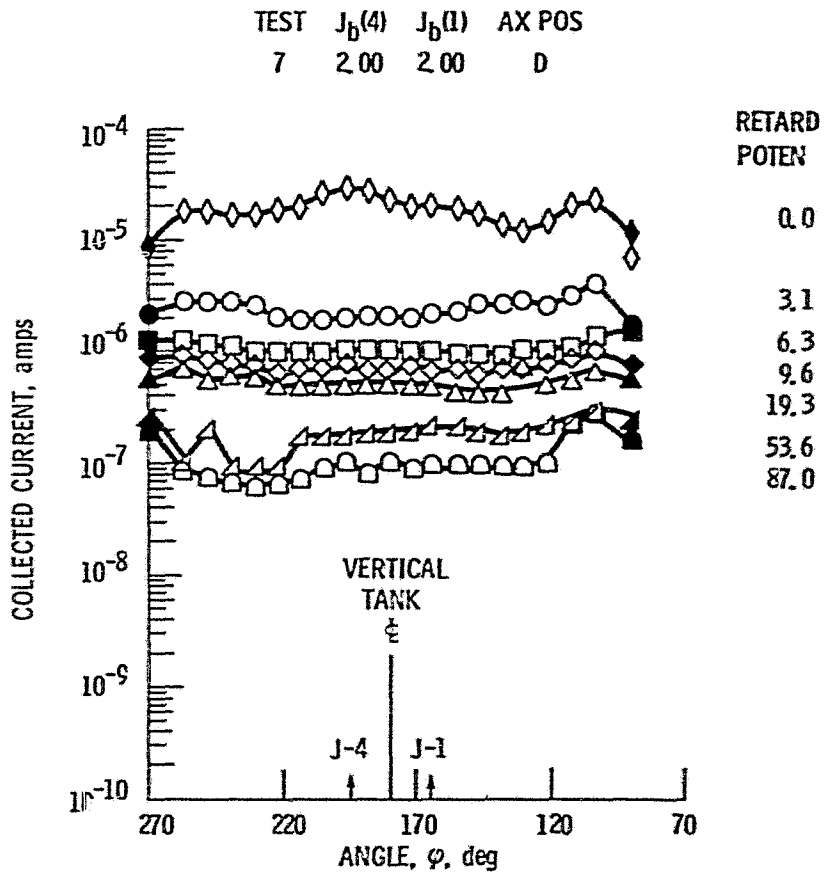

Figure 18. – Current collected by AZAX as a function of angle φ (see fig. 5) for various retarding potentials at position D.

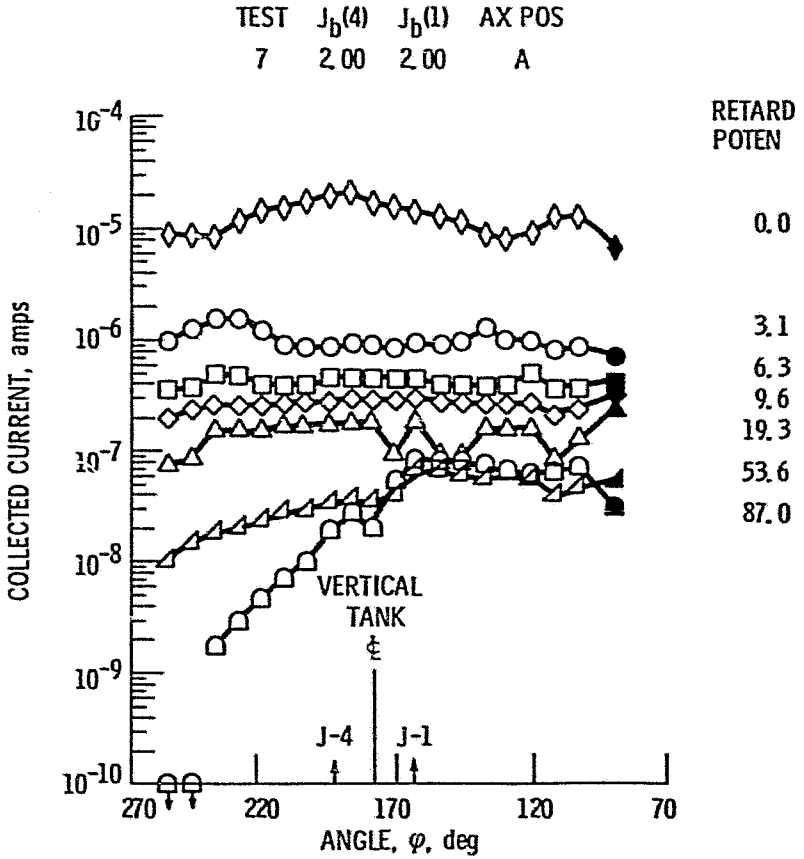

Figure 19. – Current collected by AZAX as a function of angle φ (see fig. 5) for various retarding potentials at position A.

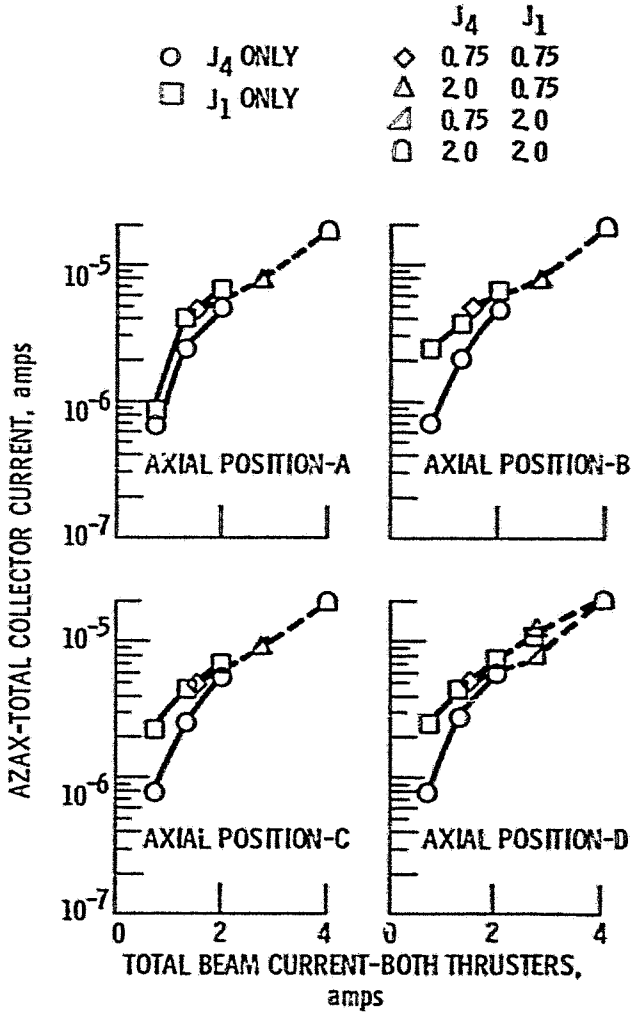

Figure 20. – Total current collected by AZAX as a function of total thruster beam current for four axial locations.

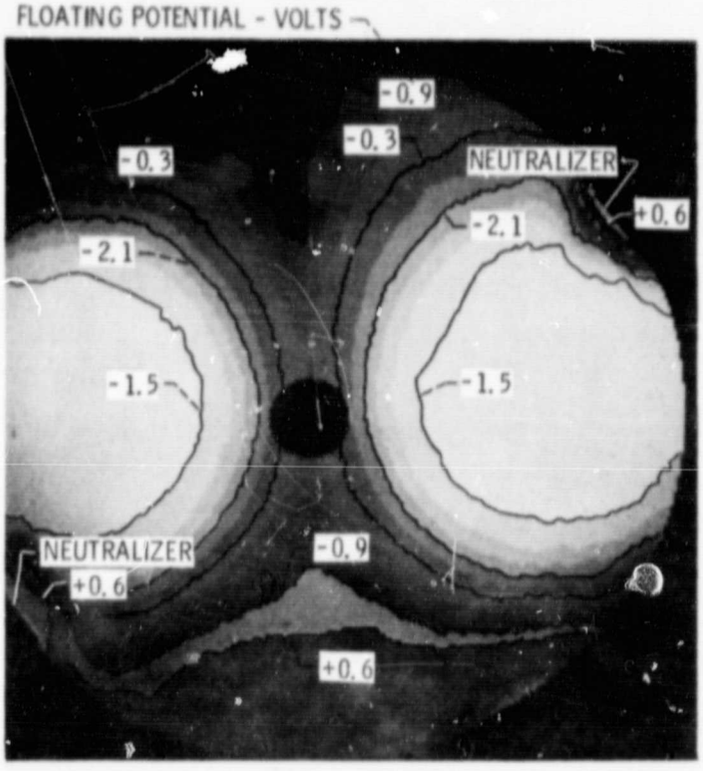

Figure 21. - Contour map of two thrusters running at 2.0 A each. Distances of planes from grids were 8.9, 14.0, 19.0, and 24.1 cm.